# The Optical, Electronic, and Electroluminescent Properties of Novel Poly(*p*-phenylene)-Related Polymers

**Marcus Remmers and Dieter Neher***

*Max-Plank-Institut für Polymerforschung, Postfach 3148, D-55021 Mainz, Germany*

**Johannes Grüner and Richard H. Friend**

*Cavendish Laboratory, Lensfield Road, Cambridge CB3 0HE, U.K.*

**Gerwin H. Gelinck and John M. Warman**

*Radiation Chemistry Department, IRI, Delft University of Technology, Mekelweg 15, 2629 JB Delft, The Netherlands*

**Calogero Quattrocchi, Doni A. dos Santos, and Jean-Luc Brédas**

*Service de Chimie des Matériaux Nouveaux, Centre de Recherche en Electronique et Photonique Moléculaires, Université de Mons-Hainaut, Place du Parc 20, B-7000 Mons, Belgium*

*Received April 23, 1996; Revised Manuscript Received July 22, 1996*[⊗]

ABSTRACT: A variety of novel, soluble, conjugated PPP- and PPV-related polymers have been synthesized using a synthetic approach that allows for the tailoring of the chemical structure of the polymer backbone. The absorption and emission properties of the materials can be tuned over a wide range of the visible spectrum. The materials were characterized in terms of molecular weight and phase behavior. The localization of the energy levels of the polymers has been determined with quantum mechanical calculations and experimentally with optical methods and cyclovoltametry. The mobilities of charge carriers measured in the microwave conductivity experiment are on the order of $10^{-7}$ $m^2/(V \cdot s)$ with an activation energy of ca. 0.06 eV. Photoluminescence (PL) quantum yields in solution are generally higher than 60%; in the solid state values even of up to 73% are observed. If the conjugation is interrupted every tenth phenyl unit, mobilities are reduced by a factor of about 2 and PL efficiences are significantly increased. A range of electroluminescent devices partly containing additional electron- and hole-transporting layers were also investigated. We obtain internal EL efficiencies of up to 4% in the blue region.

## I. Introduction

The search for new materials for light-emitting diodes (LED) based on polymers and the investigation of the various phenomena leading to the emission of light such as charge injection, charge transport, or charge recombination in organic materials turned out to be a challenge for chemical and physical research in the last few years.

One major goal in the development of materials for organic display devices is the wide tunability of emission wavelength and a high efficiency of the LED. Early polymeric devices had been based either on poly(*p*-phenylenevinylene) (PPV),[1,2] poly(*p*-phenylene) (PPP),[3,4] or polythiophene (PT),[5,6] which show emission in the green, blue, and red wavelength region, respectively. In order to achieve the emission of different colors from one polymer system, suitable substituents have been covalently linked to the polymer main chain causing a change in its electronic structure.[7] A different approach was the synthesis of copolymers with conjugated fluorescent blocks of defined length which were separated by nonconjugated spacers both into the polymer main chain or of nonconjugated polymers with fluorescent dyes in the side chains.[8−11] This allowed for a precise adjustment of emission color.

Another focus of the research activities in the field of polymer LEDs is the improvement of the quantum efficiency of both photoluminescence (PL) and electroluminescence (EL). A strong increase of device efficiency was reported using a conjugated/nonconjugated PPV-based copolymer.[12,13] This effect has been explained by trapping of the radiative exciton on the conjugated segments, hindering their migration to quenching sites. This concept was systematically studied by Braun *et al.*, who reported a strong correlation between the quantum efficiency of luminescence and the degree of conjugation for a soluble dialkoxy-substituted PPV[14] and dialkyl-substituted PPV.[13] Exciton trapping might also be the reason of the high PL and EL efficiences of partially conjugated PPV[15] and of conjugated oligomers blended into an optically inactive matrix.[16] Indeed, highly efficient LEDs based on blend polymer layers have been reported recently.[17−20]

The understanding of the mechanism leading to the improved PL and EL efficiences in copolymers is difficult, because several effects have to be taken into account. For example, the incorporation of flexible nonconjugated segments into a rigid conjugated polymer will reduce the stiffness of the backbone and therefore effect the microscopic molecular order of the polymer. This might alter the rate of interchain exciton hopping processes. In addition to this, the introduction of nonconjugated segments might increase the bandgap, if the length of the conjugated segments becomes smaller than the effective conjugation length. In this case, charges might not be injected into the polymer layer as efficiently. Therefore, the balance of charge injection is altered, too, which is one of the major prerequisites for efficient light emission.

[⊗] Abstract published in *Advance ACS Abstracts,* September 15, 1996.

S0024-9297(96)00599-2 CCC: $12.00 

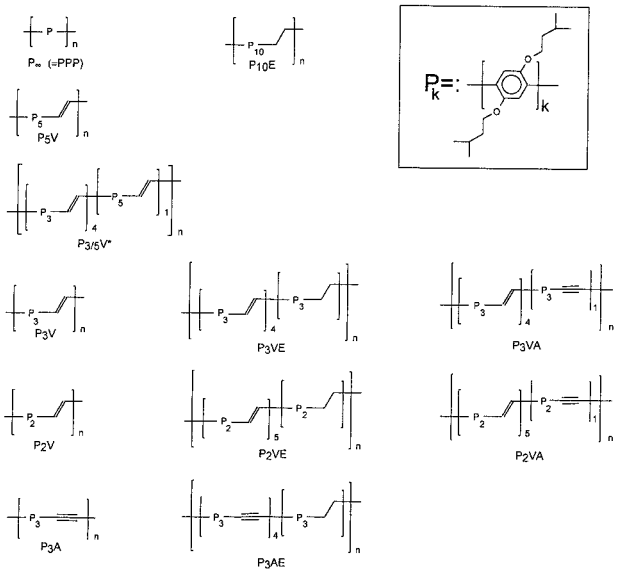


**Figure 1.** Chemical structures of new poly(*p*-phenylene)-related polymers. E.g., P3V is a homopolymer of ter-*p*-phenylene units directly connected by vinylene units. (*) Including OH functionalities in the side chains of the middle phenyl group in the P5V units.

In this paper, we present detailed investigations on the electronic and optical properties of a series of PPP-related novel homo- and copolymers. The structures of the polymers are shown in Figure 1. All of them are soluble in organic solvents like toluene, chloroform, tetrahydrofuran, or dichloromethane. Some of these materials consist of strictly alternating backbone structures like the P3A or P2V; others are statistical copolymers like the P10E or P3VE. The index at the brackets in Figure 1 indicates the ratio of the respective different repeating units. One polymer, P5V, has been synthesized in a strictly alternating type (only pentaphenylene−vinylene units) and as a statistical copolymer (mixture of ter-, penta-, and heptaphenylene−vinylene units). It can be derived, from various optical and physical methods, that the copolymerization parameters of the different comonomers during the respective polymerization reaction are identical, so that the copolymers can be considered as homogeneous.

In the following, the different polymers are named as PkXY, where Pk is the number of directly connected benzene units and X and Y indicate the linking functionalities (E = ethylene, V = vinylene, and A = ethynylene). It should be pointed out that there are a number of series of closely related materials allowing for the investigation of structure−property relations:

The PkV series (PPP, P5V, P3V, P2V, PPV) consists of strictly alternating materials. Within the series the fraction of vinylene groups in a backbone of poly(*p*-phenylene) is varied from 0 (PPP) to 0.5 (PPV). Various properties of the polymers of this series can be illustrated in plots of any property against the molar fraction of vinylene units in the backbone. Similar relations can be considered for the PkA series. Here the fraction of ethynylene units in the backbone of PPP polymers is varied (PPP, P3A). All PkV and PkA polymers are fully conjugated polymers of rigid rod type due to their stiff backbone. For most of them a counterpart in the PkVE or PkAE series was synthesized. These materials are basically identical with the PkVs and PkAs except for the fact that after statistically about 12 phenylene units the vinylene or ethynylene unit is exchanged into an ethylene unit. The latter causes an interruption of the conjugation along the backbone and at the same time introduces a flexible unit into the rigid rod.

Also the P3VA and P2VA polymers are closely related to P3V and P2V. They contain a small amount of ethynylene units in the P3V or P2V backbone. This variation causes a local change in the electronic structure of the polymers, but it preserves the conjugation along the backbone and its rigidity. The P3/5V is related to the P3V in a similar way, too. In this polymer a small amount of pentaphenylene−vinylene units is introduced into a polymer backbone consisting of 80% terphenylene−vinylene units. The described matrix of new materials allows the study of different structure variations on the properties of the material: e.g., the fraction of vinylene or ethynylene units can be varied (PkV series, PkVE series) as well as the linking functionality between, e.g., terphenylene units (P3V, P3VE, P3VA, P3/5V).

The comparison of the different materials within one series allows for the investigation of various structure−property relationships such as phase behavior, absorption or emission spectra, or electronic properties. Charge injection and charge transport properties will be discussed by comparing emission color and quantum efficiencies of devices with single-layer and triple-layer device geometry, using emissive polymers with different positions of the HOMO and LUMO states. The investigation of electroluminescent devices particularly offers a new possibility of probing the energy spectrum of the different polymers, in a way such as "optical spectroscopy", because it is a powerful tool of determining low lying states in very low concentrations. This is helpful for the understanding of red-shifted emitters or trapping.[21,22]

## II. Experimental Section

**Polymer Synthesis and Characterization.** The polymers were synthesized analogous to the way described in ref 23 using the Suzuki coupling method. This method is a well-known polymerization reaction for benzene monomers generating a phenyl−phenyl link from an aromatic bromide and an aromatic boronic ester by a Pd complex-catalyzed coupling. The preparation of polymers containing oligo(*p*-phenylene) units connected by various functionalities was made possible by extending the Suzuki reaction to stilbene, diphenylethynylene, and 1,2-diphenylethane derivatives. Combination of the different AA/BB type monomer systems in various concentrations allows a tailoring of the polymer backbone structure leading to the materials shown in Figure 1. In order to provide solubility of all described materials, branched side chains such as isopentoxy groups have been attached to the monomer units. Number degrees of polymerization of up to $X_n = 137$ (osmosis) have been reached under optimized conditions.

UV spectra were measured on a Perkin-Elmer Lambda 9 spectrophotometer, photoluminescence spectra were obtained with a Fluorolog 2 Type F212, SPEX USA spectrometer with a Xe XBO 450W (Osram) lamp. Quantum yields in solution were determined twice. 9,10-Diphenylanthracene and 1,1,4,4-tetraphenylbutadiene have been used as standards. The measurements were averaged. The photoluminescence quantum yields in the solid state were determined as absolute values in an integrating sphere. Differential scanning calorimetry measurements were carried out under nitrogen with a heating rate of 10 K/min on a Perkin-Elmer DSC7 instrument. Gel-permeation chromatography (GPC) curves were obtained with THF as solvent, and molecular weights were calculated versus polystyrene standards. Membrane osmometry was performed in toluene with a Knauer osmometer at a temperature of 25 °C, using a coated acetate membrane with

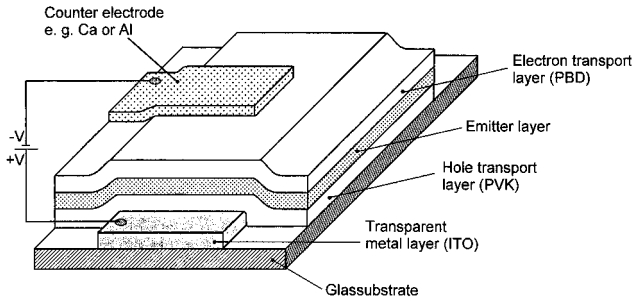


**Figure 2.** Electroluminescent device in triple-layer configuration (glass/ITO/PVK/polymer/PBD in PMMA/Ca or Al). In the different configurations reported, the charge-transport layers are not always present.

a pore size of 20 000 daltons. Cyclic voltammograms were recorded at a scan rate of 20 mV/s and performed with a potentiostat/galvanostat EG&G PAR Model 173 in $CH_2Cl_2$ solutions with a polymer concentration of $1 \times 10^{-3}$ mol of monomer units/L and *tert*-butylammonium perchloride (0.1 mol/L) as electrolyte.

**Electroluminescent Devices.** The typical device structure is shown in Figure 2. For the preparation of light-emitting diodes, glass substrates coated with indium tin oxide (ITO) with a conductivity of about 30 Ohm/square (Balzers-UK, 256) served as bottom electrodes. They were cleaned with acetone and propan-2-ol in an ultrasonic bath. To build up the monolayer devices, the respective polymers were spin-coated from toluene or chloroform. For the multilayer devices, the respective layers were deposited onto the substrates on top of each other. Poly(vinylcarbazole) (PVK, Aldrich) served as hole-transport layer (HTL) and was spin-coated from chloroform, whereas 2-(4-biphenylyl)-5-(4-*tert*-butylphenyl)-1,3,4-oxadiazole (PBD, Aldrich) in a matrix of 25 wt % poly(methyl methacrylate) (PMMA, Aldrich) was employed as electron-transport layer (ETL). The latter was spin-coated from acetone solution. The solutions were filtered through a 0.45 $\mu$m filter. The respective layer thickness was defined by using an appropriate spinning speed and concentration of the polymer solution. Typical film thicknesses ranged from 90 to 150 nm (Dektak II stylus profilometer). Top contacts of about 100 nm calcium or aluminum were deposited by vacuum evaporation at pressures of less than $10^{-5}$ Torr at rates of about 0.5−1 nm/s. Calcium electrodes were subsequently covered with a protective aluminum layer. The active area of the device was approximately 4 $mm^2$. Subsequent processing and measurement were carried out in a nitrogen atmosphere ($O_2$ and $H_2O$ concentration less than 10 ppm) or in vacuo, at room temperature.

The current−voltage characteristics of the devices were measured in forward bias configuration with the ITO electrode at positive potential. The device voltage was increased in steps of 0.5 or 1 V with a computer controlled voltage source (Keithley 230), and the device current (Keithley 195) and the output of the photodiode (Keithley 195A) were simultaneously recorded after a delay time of about one to several seconds. This procedure was typically repeated several times for each device. The electroluminescence intensity was recorded through the transparent ITO electrode with a photodiode (RS 303−674). By considering corrections for emission characteristics, sensitivity and solid angle of the photodiode, stray light, and losses in the glass substrate, the internal electroluminescence quantum efficiency and the total light flux could be calculated from the forward emission intensity according to Greenham *et al.*[24] Spectral data were taken using a single grating monochromator with an UV-enhanced CCD camera (Oriel Instaspec IV). All data were taken at a pressure of less than 0.1 mbar. The luminescence spectra can be expressed in color coordinates defined by the Commission International d'Eclairage (C.I.E.). These are based on the fact that the average color vision of the human eye can be described by three coordinates, which define a two-dimensional representation of the color spectrum (see Figure 16). The coordinates corresponding to chromophores are a function of spectral position and profile. They can be interpreted as a measure of its purity, i.e., the range of colors, which can be generated by color addition. It therefore defines one of the requirements for the application of chromophores in commercial color displays.

For organic light-emitting devices the similarity of the luminescence−voltage and the current−voltage characteristics (see Figure 4) is consistent with the generation of the EL by recombination of opposite charge carriers. The similarity of EL and PL spectra suggests that this recombination leads to excitonic-type excitations.[1] Assuming that the amount of triplets formed is only a function of spin statistics and that any transfer of excitation energy from triplets to singlet can be neglected, the total light flux $L$ generated in the device is given by:

$$L = (\alpha\beta\eta_{PL})(r)(j_{minor}) \quad (1)$$

$\alpha$ is a proportionality constant and $\beta$ the spin statistics factor set to 0.25. $\eta_{PL}$ is the PL efficiency, and $j_{minor}$ and $j_{major}$ describe the current density of the minority and majority charge carrier flowing into the device. $r$ describes the recombination probability for a minority charge carrier. The onset voltage for electroluminescence therefore typically coincides with the onset voltage for the injection of a minority charge carrier,[25] which in PPV and PPP derivatives are typically formed by electrons.[26] It therefore represents an indicator for the injection and transport of electrons in these materials. The internal EL efficiency $\eta_{EL,intern}$ can then be expressed by:

$$\begin{aligned}\eta_{EL,intern} &= L/[(1-r)(j_{minor}) + j_{major}] \\ &= [(\alpha)(0.25)(\eta_{PL})(r)]/[(1-r) + j_{major}/j_{minor}] \\ &= [(\alpha)(0.25)(\eta_{PL})] \times f(\mathrm{el}) \end{aligned} \quad (2)$$

Therefore, the EL efficiency is most sensitive to the charge-carrier balance, and the relative change of the efficiency is equally sensitive to the relative change of $j_{minor}$ and $j_{major}$. The parameter $f$(el) is a function of injection, transport, and recombination of charge carriers and describes the efficiency for the conversion of minority charge carriers into optical excitations. In summary, the comparison of the EL and PL data provides additional information about the current distribution in the device. Especially the effect of additional charge-transport layers on the device performance can be investigated.

Although generated from the same excited state, EL and PL probe the organic layer in different ways. The spatial distribution of emitters generated in a PL experiment is given by the absorption profile of the excitation source followed by possible energy-relaxation processes.[27] In an EL experiment, however, the recombination is preceded by the migration of the opposite charge carriers through the film, which can result in a preferred emission from trapping sites and regions of higher conductivity. Additionally, charge carriers are subjected to the energy dispersion of the hopping sites.[27] Recently, the large difference in the spectral location of photoluminescence and electroluminescence had been assigned to the trapping of injected charges.[21]

The EL characteristics of polymer light-emitting devices have been found to be sensitive to the formation of additional chromophores in organic materials, such as aggregates,[22] or have been used to investigate the spatial distribution of the charge-carrier recombination zone.[28,29]

**Pulse-Radiolysis Time-Resolved Microwave Conductivity Measurements (PR-TRMC).** Samples for measurements of the conductive properties of the materials by PR-TRMC are prepared by compressing dry polymer fibers into a rectangular cell using a close-fitting Teflon rod. The cell is closed at one end and has an inner cross section of 3.55 and 7.1 mm. The sample length, of approximately 10 mm, and weight (ca. 150 mg) are accurately measured. The cell is placed in a cryostat in which the temperature can be varied from −100 °C up to +200 °C. The samples were irradiated with 2−50 ns pulses of 3 MeV electrons from a Van de Graaff accelerator. The total beam charge in the pulse $Q$ was monitored by deflection onto a 50 W coaxial target. The energy

**Table 1. Molecular Weight and Phase Behavior of Polymers**

| polymer | $M_n$ (GPC:[a] THF) | $M_w$ (GPC:[a] THF) | $P_n$[b] (GPC) | $D$ | $M_n$ (osmosis, toluene) | $P_n$ (osmosis, toluene) | $T_g$ (°C) | mp (°C) |
|---|---|---|---|---|---|---|---|---|
| PPP | 50 000 | 130 000 | 202 | 2.6 | 34 000 | 137 | 20 | 190 |
| P5V | 30 600 | 71 100 | 48 | 2.3 | nd[c] | – | 20 | –[d] |
| P5Vstat | 105 400 | 544 300 | 333 | 5.2 | nd[c] | – | 20 | –[d] |
| P3/5V | 109 000 | 465 000 | 93 | 4.3 | 50 000 | 42 | 30 | 195 |
| P3V | 168 000 | 573 000 | 143 | 3.4 | nd[c] | – | 40 | 215 |
| P2V | 21 000 | 51 000 | 40 | 2.4 | nd[c] | – | 40 | –[d] |
| P3A | 25 000 | 213 000 | 65 | 8.5 | 27 000 | 67 | 30 | –[d] |
| P10E | 22 000 | 141 000 | 79 | 6.4 | nd[c] | – | 20 | –[d] |
| P3VE | 13 900 | 48 000 | 36 | 3.5 | 7 400 | 19 | 30 | 205 |
| P2VE | 12 200 | 35 600 | 23 | 2.9 | nd[c] | – | 43 | 235 |
| P3AE | 15 800 | 54 900 | 42 | 3.5 | nd[c] | – | – | –[d] |
| P3VA | 11 300 | 43 800 | 29 | 3.9 | nd[c] | – | 35 | –[d] |
| P2VA | 19 300 | 240 000 | 37 | 12.4 | nd[c] | – | – | 252 |

[a] Standard: polystyrene. [b] Average according to comonomer composition. [c] nd = not determined. [d] No peak detected in DSC experiment.

deposition per unit volume within the sample was found to be $D = 540$ J/m$^3$ per 1 nC of beam charge. The penetration depth of the primary 3 MeV electrons in these materials is approximately 15 mm, so the energy can be taken to be deposited uniformly within the 3.55 mm thick sample. The energy dissipated along the track of a primary electron produces electron−hole pairs with a distance between the energy deposition events of, on average, 2000 Å or more. The ionizations will occur with close to equal probability per unit volume in the conjugated backbone and hydrocarbon regions of the material. No radiation damage, apparent as either a change in signal height or decay kinetics, was found during the course of the measurements. Microwaves are used to monitor any change in the conductivity of the medium on pulsed irradiation. Measurements are made in the 26.5−38 GHz region. For small changes in the reflected microwave power, $P$, the microwave loss, $\Delta P$, is directly proportional to the radiation-induced conductivity change, $\Delta\sigma$:

$$\Delta P/P = -A(\Delta\sigma) \tag{3}$$

where $A$ is determined using computational and data-fitting procedures.[30] The TRMC technique is fully described elsewhere.[30,31]

**Theoretical Methodology for Quantum Mechanical Calculations.** The geometry of PPP, as well as that of P2V, P3V, and P5V polymers (see Figure 1), were obtained by means of the semiempirical Hartree−Fock Austin Model 1 (AM1) technique which was designed to reproduce accurate geometries and heats of formation, particularly for organic compounds.[32] The choice of the AM1 method is further appropriate in this case since the calculated geometry and the experimental data of the poly(*p*-phenylenevinylene) (PPV) dimer present a good agreement.[33] Due to the large size of the alkyl substituents in the synthesized systems, we have introduced methoxy groups in the 1,4 position of the phenyl rings. This approximation is justified by the fact that the size of substituents does not play a role in modifying the geometry of the rings and in the electronic properties as well. The AM1 optimizations are performed at the polymer level using the MOPAC 93 package running on a IBM RISC/6000 workstation.

On the basis of the AM1 structural data, we determine the most relevant electronic parameters of the polymers (bandgap, ionization potential, and electron affinity) for VEH ("valence effective Hamiltonian") band structure calculations and compare to the experimental values. This technique is well-known to provide reliable estimates for the electronic properties of conjugated and nonconjugated polymers.[34,35]

## III. Results

**Polymer Properties.** All polymers are colorless to yellow fibrous materials, dissolving in common organic solvents like toluene, THF, or chloroform. The molecular weights were determined by GPC and osmosis and are displayed in Table 1. It is well-known that poly(*p*-phenylene)-type molecules exhibit a certain persistence.[36] In order to provide solubility of these polymers, flexible side chains have been attached to the polymer backbone.[37] Recently, the expression "hairy rod molecules" has been introduced for this type of polymers.[38] Due to the different Mark-Howing factor of such rodlike molecules, the molecular weights determined by GPC can be expected to be too high and the dispersities to be too broad. This effect is confirmed by the $M_n$ values measured by osmosis, which are generally smaller than $M_n$ determined by GPC by a factor of 0.5−0.7.[36,39] Polymers with extremely high dispersities according to GPC are expected to be adsorbed to the column or show aggregation effects. In any case even the polymers with the lowest molecular weights have contour length of at least 12 nm corresponding to about 30 phenyl units ($M_n$) which is still beyond the conjugation length of these materials.[40] Therefore, the observed optical properties of all polymers are not influenced by the molecular weights of the different compounds.

All materials show similar phase behavior: A weak $T_g$ is found between 20 and 40 °C. This can be attributed to a side chain melting process. Between 190 and 250 °C the polymers melt to form a liquid crystalline phase. An isotropization is not observed for any polymer before decomposition which starts at temperatures of 320 °C (onset of weight loss in the thermogravimetric experiment). An accurate characterization of the anisotropic liquid phases is difficult, because the polymers tend to exhibit degradation processes at high temperatures. Especially the materials containing vinylene and ethynylene units seem to undergo irreversible crosslinking reactions[41,42]—in some cases even before the melting. This is the reason why for some polymers no melting peak can be observed in the DSC experiment (see Table 1). The chemical and structural changes upon heating can affect the electronic properties of the polymer (see below). A more detailed investigation of the mesophases of PPP, which does not contain any vinylene or ethynylene units, is reported elsewhere.[43,44]

Comparing the different series of polymers, one observes that both $T_g$ and melting point increase upon increasing molar fraction of vinylene groups of the PPP backbone ($T_g$: PPP 20 °C, P2V 40 °C; melting: PPP 190 °C, P2V > 220 °C). These trends can be understood in terms of a change in the side chain density along the polymer main chain. PPP has the highest side chain density (2 side chains per 4.2 Å contour length; density: 1 chain/2.1 Å) whereas the P2V exhibits the lowest (4 side chains per 10.7 Å; density: 1 chain/2.7 Å). Phase transition temperatures of hairy rod molecules are mainly determined by the gain of entropy during the transition, which is related to the number of possible

**Table 2. Absorption, Emission, and PL Efficiency in the Solid State, Extinction of Polymers**

| polymer | abs $\lambda_{max}$ (nm) (film) | abs $\lambda_{max}$ (nm) (in $CH_2Cl_2$) | em $\lambda_{max}$ (nm) (film) | em $\lambda_{max}$ (nm) (in $CH_2Cl_2$) | PL eff in the solid state (%) (±10%)[a] | PL eff in solution (%) (±10%)[a] | extinction (L mol$^{-1}$ cm$^{-1}$)[b] |
|---|---|---|---|---|---|---|---|
| PPP | 336 | 335 | 401 | 401 | 34 | 59 | 8 900 |
| P5V | 380 | 385 | 446 | 448 | 49 | 47 | 9 100 |
| P5Vstat | 381 | 390 | 448 | 449 | 69 | 49 | 9 200 |
| P3V | 391 | 400 | 460 | 445 | 9 | 54 | 15 400 |
| P3/5V | 387 | 390 | 460 | 445 | 40 | 57 | 12 500 |
| P2V | 407 | 415 | 480 | 470 | 9 | 56 | 17 300 |
| P3A | 375 | 378 | 452 | 424 | 25 | 60 | 14 800 |
| P10E | 331 | 331 | 441 | 395 | 73 | 54 | 7 500 |
| P3VE | 389 | 396 | 458 | 451 | 45 | 58 | 11 100 |
| P2VE | 399 | 403 | 475 | 470 | 61 | 62 | 14 200 |
| P3AE | 371 | 376 | 445 | 424 | 33 | | 10 200 |
| P3VA | 388 | 389 | 478 | 452 | 40 | 44 | 12 300 |
| P2VA | 406 | 413 | 476 | 476 | 35 | 66 | 16 700 |

[a] Relative error. [b] Calculated per mole of phenyl units.

conformations of the polymer. Since the rigid backbone does not gain any further conformations at a solid−liquid-phase transition, the gain of entropy is determined by the density of side chains.[45] Also a change in the persistence of the backbone might influence the melting point.

Similar considerations explain why the melting point in the PkVE series is lowered in comparison to the fully conjugated materials (215 °C (P3V) toward 205 °C (P3VE)). If flexible segments are introduced into the conjugated backbone, the macromolecule gains a lot more possible conformations in the liquid phase during melting. Therefore, the phase transition entropy is increased and consequently the melting point decreased. If stiff units like ethynylene groups are introduced into a PkV polymer (PkVA series), the rigidity of the backbone is not significantly altered and the melting point not effected.

The stability of the reported polymers in the solid state or in solution is generally very high if stored cool and dark. Exposure to light in connection with atmospheric oxygen leads to slow degradation. Detailed investigations on the mechanism will be reported elsewhere.

**Optical Properties.** Depending on the type of link between the oligo(*p*-phenylene) units and their sequence length, both the absorption and emission properties of the resulting polymers can be tailored (Table 2). The PkV, PkA, and PkVA polymers are examples of fully conjugated aromatic polymers, whereas PkE, PkVE, and PkVA contain interruptions of the conjugation of the backbone. The statistical sequence length of conjugated segments is 10−15 in the various polymers, which is about the reported conjugation length of polyphenylene-type polymers.[40]

As expected from the low concentration of nonconjugated segments, the absorption and emission properties of the polymers with broken conjugation do not differ significantly from their fully conjugated counterparts, but other optical properties like the photoluminescence quantum yields in the solid state do change dramatically. The absorption and emission maxima in solution and in the solid state as well the photoluminescence quantum yields and extinction coefficients are given in Table 2.

The absorption maxima in the film are generally slightly blue-shifted compared to the maxima in solution ($CH_2Cl_2$) whereas the emission from the solid state is red-shifted compared to the values in solution due to energy migration and relaxation processes.

The emission maximum of P10E can be expected at approximately 385 nm (3.14 eV), which is the emission maximum of an analogous substituted decaphenylene molecule.[46] This is in fact observed for P10E in dilute solutions. However, the maximum emission in the solid state is strongly red-shifted (441 nm, 2.81 eV). This effect is due to impurities in the polymer backbone (<5% vinyl units instead of ethane units from residual stilbene in the monomers used in the polymerization). These few vinylene units in the material serve as very efficient traps for the mobile excitons. Therefore, a large percentage of the light is emitted from the vinylene groups. This kind of efficient energy transfer is not possible to the same extent in dilute solution, and the emission maximum is situated at 395 nm with a small shoulder at 440 nm. The fluorescence lifetime at the maximum determined by laser flash photolysis is 0.74 ns whereas the fluorescence lifetime at 440 nm is ca. 1 ns.[47] This result is further evidence that the emission band at 440 nm originates from the few stilbene units in the P10E backbone. These impurities also affect the performance in electroluminescent devices (see below).

Another material exhibiting an unusual behavior is P3VA. This polymer is very closely related to P3V, with the only difference that statistically every fourth vinylene group is replaced by an ethynylene unit. It can be expected that this slight difference does not alter the spectral position of the absorption or emission maxima, as it is observed in P2V ($Abs_{max}$: 407 nm) and P2VA ($Abs_{max}$: 406 nm). However, the solid state emission of P3VA is strongly red-shifted compared to the value measured in solution. This indicates that the excitation energy is transferred to structural defects of lower energy. From here, red-shifted light is emitted or the excitons decay nonradiatively. The latter is reflected by the low quantum efficiency in the solid state of only 10%. From the ratio of quantum yields of P2V (12%) and P2VA (35%) one would expect a value of approximately 30% for the PL efficiency of P3VA.

We have further investigated two very similar "P5V" polymers: one strictly alternating poly(penta-*p*-phenylene−vinylene) ("P5V") and one statistical copolymer containing various lengths of oligo-*p*-phenyls between the vinylene units with an average length of five ("P5Vstat"). The absorption and emission properties of these materials are very similar; however, the quantum yields in the solid state are quite different.

**Electroluminescence.** Figure 3 shows a typical I−V curve under forward bias condition, which follows an exponential-like profile. The EL intensity is a linear function of the current. These findings are consistent

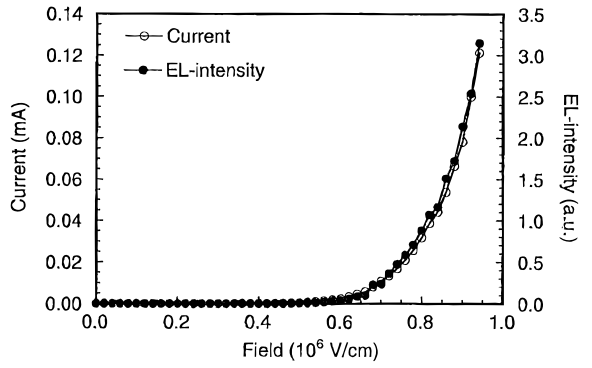


**Figure 3.** Current and light output against voltage of a triple-layer device (configuration: glass/ITO/PVK/PPP/PBD in PMMA/Ca).

with earlier studies of polymer light-emitting devices.[1,25] The device efficiencies achieved range from less than 0.01% for PPP single-layer devices to 4% for devices made of P3/5V, which contain an additional hole-transport layer (HTL) and electron-transport layer (ETL) (see Table 3). Deep blue emission is achieved from PPP multilayer devices with an efficiency of about 1%.

The trends in EL efficiency for single- and multilayer devices of the respective polymers are comparable, but the currents through the devices at a given external field are significantly reduced in multilayer devices. The field for light onset is reduced for most of the devices with an additional charge-transport layer. Polymers with higher bandgaps generally exhibit smaller currents. Devices with aluminum top electrodes show a reduced device efficiency while the current for a given external field is not affected.

The EL spectra of most polymers were very similar to the corresponding PL spectra in solid state. However, some deviations of EL and PL could be observed depending on the device configuration, the electrode material, and the operation time of the device. If an ETL is present, the EL spectra are generally similar to the PL. Single layer devices or devices with an HTL show a varying degree of an additional red-shifted emission. After longer driving times, some devices showed an increased red emission. A special case was found for P3A (Figure 4). In this material a very strong red shift is observed in all device configurations with a calcium−polymer interface. This red shift is less pronounced in similar devices with aluminum as counter electrode.

**PR-TRMC Results.** Irradiation of all of the polymers studied gave readily measurable conductivity transients. All transients displayed a short-lived ($t \leq$ 1 ns) component which saturates in the pulse and a long-lived signal which decayed on a time scale longer than the pulse duration. The afterpulse first half-life was typically tens of nanoseconds. However, because of the very disperse (nonexponential) nature of the decays, a substantial transient conductivity still remained on a time scale of many microseconds. These observations are illustrated by results for P3V in Figure 5. In Table 4 the end-of-pulse conductivities per unit dose, $\Delta\sigma_{eop}/D$, for the long-lived component and the first half-lives are listed.

For the majority of compounds the short-lived, in-pulse component was very small and similar in magnitude to a spurious transient observed for other materials. For PPP, however, it was significantly larger and is thought to indicate possibly the initial formation of a highly mobile charge carrier which becomes trapped in a time of approximately 1 ns. The conductivity due to this short-lived carrier is estimated to be approximately 1 order of magnitude larger than the end-of-pulse conductivity of the long-lived component given in Table 5.

For PPP, P2V, and P3V the temperature dependence of the radiation-induced conductivity was measured, and $\Delta\sigma_{eop}/D$ is plotted as a function of temperature in Figure 6 for PPP and P3V. A gradual increase in $\Delta\sigma_{eop}/D$ is found on heating. On cooling, $\Delta\sigma_{eop}/D$ decreases, but remains higher than during heating. The room temperature value of $\Delta\sigma_{eop}/D$ after heating to ca. 155 °C has increased by ca. 50% and 40% compared with the fresh samples for PPP and P3V, respectively (Table 6). On further cooling, $\Delta\sigma_{eop}/D$ tends to reach a plateau. In terms of an overall activation energy, the temperature dependence found on cooling corresponds to $E_A = 0.07$ eV for PPP and $E_A = 0.05$ eV for P3V. For P2V, a similar temperature dependence is observed. The only difference is that no annealing effect is found for P2V.

For P5V, the conductivity also initially increases on heating but tends to plateau out at about 150 °C. The conductivity remains low on returning to room temperature. This is consistent with the DSC results which showed no melting peak for P5V and is probably a result of the occurrence of cross-linking at elevated temperatures. This clearly has a marked negative influence on charge carrier motion.

**Quantum Mechanical Calculations.** The polymer unit cells of PPP, P2V, P3V, P5V, and P3A were optimized at the AM1 level. In PPP and PkV polymers, the phenyl rings rotate around the inter-ring bonds in order to prevent the steric interactions between hydrogens and the methoxy side groups on adjacent rings. We have assumed that in PPP, P3V, and P5V the adjacent rings rotate in opposite directions, which means that every other phenylene ring lies within a common plane, as reported on the basis of X-ray diffraction data on PPP oligomers.[48] We have obtained a ("gas phase") value of ca. 44° for the dihedral angle between adjacent rings in the AM1 geometry optimizations performed for PPP, P3V, and P5V polymers, which is in agreement with the analysis of X-ray diffraction data of single crystals of model compounds.[49] The vinylene moieties are found to lie in the same plane as that of their neighboring phenylene rings in P3V and P5V, which results in the appearance of planar dimethoxy-substituted stilbene units along the polymer backbone. In P2V this possibility is ruled out, since there is a large steric hindrance against the planarity of the two phenylene rings in the unit cell; in this polymer the vinylene group is calculated to be about 6° out of the plane of one of the phenylene rings of the unit cell and 35° out of the plane of the other ring, the dihedral angle between the two phenylene rings in the unit cell being around 41°.

In Table 7, we report the calculated VEH bandgap ($E_g$), as well as the solid state electron affinity (EA) and ionization potential (IP) for various polymers considered in this study. We note that the bandgap increases going from P2V (2.75 eV) to P5V (2.94 eV), i.e., with the number of phenylene rings in the polymer unit cell. In fact, PkV compounds can be considered as dimethoxy-PPV/PPP block copolymers; the PkV electronic parameters are then estimated to be comprised between those of the parent polymers. Note that we have obtained bandgap values of 2.07 and 3.46 eV for dimethoxy-PPV (DMeOPPV) and PPP, respectively. This study can be

**Table 3. Electroluminescence Data in Different Device Configurations (Emission Maximum, Onset Voltage, Efficiency)**

| | monolayer (ITO/Pol/Ca) | | | bilayer (ITO/PVK/Pol/Ca) | | | triple layer (ITO/PVK/Pol/PBD[a]/Ca) | | | monolayer (ITO/Pol/Al) | | |
|---|---|---|---|---|---|---|---|---|---|---|---|---|
| polymer | $\lambda_{max}$ (nm) | onset (MV/cm) | eff (%) | $\lambda_{max}$ (nm) | onset (MV/cm) | eff (%) | $\lambda_{max}$ (nm) | onset (MV/cm) | eff (%) | $\lambda_{max}$ (nm) | onset (MV/cm) | eff (%) |
| PPP | 450 | 3.2 | 0.01 | | 1.3 | 0.16 | 423 | 0.44 | 0.6 | | 1.5 | 0.01 |
| P3V | | 0.94 | 0.04 | | 0.82 | 0.10 | 464 | 0.83 | 0.4 | | | |
| P3/5V | | 1.2 | 0.24 | | 0.44 | 0.13 | 459 | 0.69 | 4.0 | | 2.4 | 0.02 |
| P2V | 483 | 1.3 | 0.06 | | | | 486 | 0.50 | 2.0[b] | 482 | 1.7 | 0.02 |
| P3A | | 1.0 | 0.3 | | 0.5 | 0.2 | 650 | | | | | |
| P10E | 452 (400) | 1.4 | 0.1 | 450 | 1.5 | 0.09 | 450 | 0.70 | 1.0 | 450 | 2.1 | 0.10 |
| P3VE | | | | 464 | 0.75 | 0.15 | 463 | 0.54 | 1.4 | | | 0.12 |

[a] 25 wt % in PMMA. [b] No PVK.

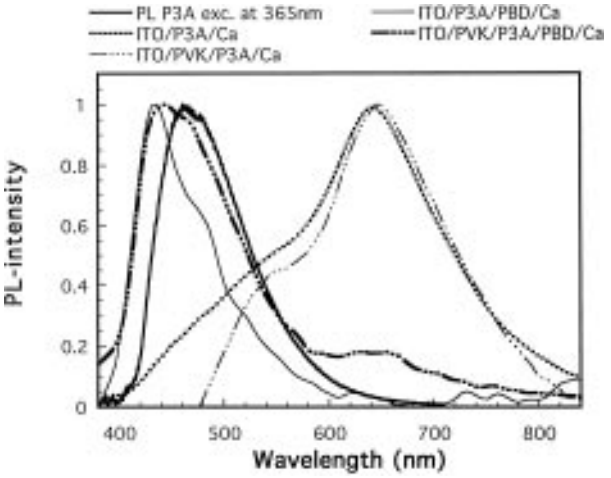


**Figure 4.** Electroluminescence and photoluminescence spectra of P3A in various configurations. Electroluminescence from a double-layer structure (ITO/PVK/P3A/Ca) and a triple-layer device configuration (ITO/PVK/P3A/PBD/Ca) in comparison to photoluminescence of P3A and the emission of an electroluminescent double-layer structures without P3A (ITO/PVK/PBD/Ca).

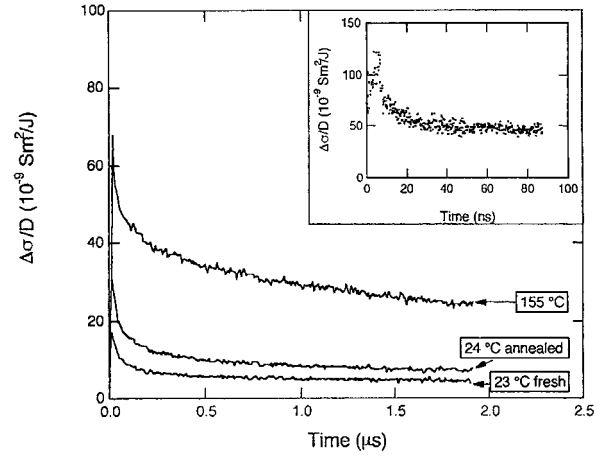


**Figure 5.** Dose-normalized radiation-induced conductivity transients obtained at room temperature for P3V freshly precipitated, at 155 °C, and at room temperature after annealing at 155 °C. Inset: TRMC transient for the first 100 ns obtained at 155 °C using a 10 ns pulse.

related to previous works on the electronic structure of PPP/polyacetylene (PA) copolymers;[50] these have shown that the evolution of the electronic parameters in stereoregular PPP/PA chains is linear with respect to the concentration in one of the homopolymer repeating units;[51] whereas deviations from the linear evolution are found in nonregular (random) chains.[52] The results obtained for the PkV polymers indicate a deviation from the linear evolution of the bandgap with respect to the molar fraction of vinylene groups (see Figure 8); this

**Table 4. Calculated Values for *f*(el) of Different Compounds and Device Configurations**

| compd | *f*(el) single layer (%) | *f*(el) triplet layer (%) |
|---|---|---|
| PPP | 0.12 | 7.3 |
| P10E | 0.55 | 0.55 |
| P3V | 1.8 | 18 |
| P3VE | 1.3 | 12 |
| P35V | 2.4 | 40 |
| P3VA | 3.0 | |
| P2V | 2.6 | 87 |
| P3A | 4.8 | |
| PPV | 40 | 80 |

**Table 5. Dose-Normalized End-of-Pulse Conductivities, Charge-Carrier Pair Formation Energy, and Lower Limit of the Sum of the Charge-Carrier Mobilities for the Long-Lived Signals of the Fresh Samples at Room Temperature**

| compd | $\Delta\sigma_{eop}/D$ ($10^{-9}$ Sm²/J) | $E_p$ (eV) | $\sum\mu_{min}$ [$10^{-8}$ m²/(v·s)] | first half-life[b] (ns) |
|---|---|---|---|---|
| PPP[a] | 5.0 | 17 | 8.5 | 30 |
| P5V | 8.2 | 15 | 12.3 | 110 |
| P3V | 17.0 | 14 | 23.8 | 60 |
| P2V | 2.5 | 14 | 3.5 | 20 |
| P10E | 2.0 | 17 | 3.4 | 30 |
| P3VE | 5.0 | 14 | 7.0 | 90 |
| P2VE | 2.0 | 14 | 2.8 | 40 |
| P5Vstat | 4.4 | 15 | 6.6 | 120 |
| P35V | 4.0 | 14 | 5.6 | 40 |
| P3A | 5.5 | 14 | 7.7 | 220 |

[a] Evidence was found for a short-lived, ca. 1 ns, component with $\Delta\sigma_{eop}/D$ approximately a factor of 10 larger than the slowly decaying component. [b] Due to the very disperse decay kinetics a substantial conductivity signal is still present on a microsecond timescale as shown in Figure 5.

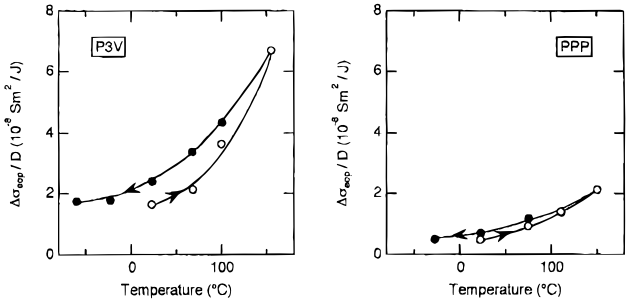


**Figure 6.** Temperature dependence of the dose-normalized conductivity of the long-lived component for P3V (left) and PPP (right). Open circles are measurements obtained on heating, and closed circles are measurements obtained on cooling.

has to be related to their geometric structure, in particular the lack of planar dimethoxystilbene units along the P2V backbone, in contrast to the situation in P3V and P5V. We note from Figure 8 that there is an overall very good agreement between the theoretical

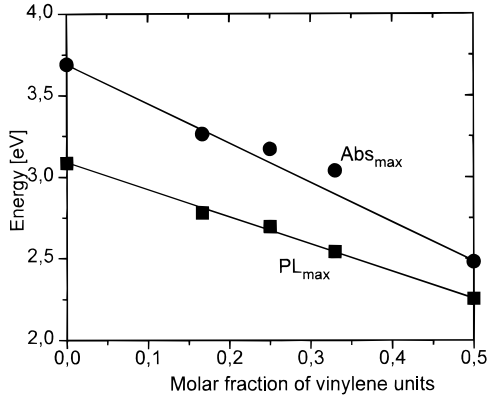


**Figure 7.** Absorption and emission maxima of PkV polymers plotted against the molar fraction of vinyl groups in the backbone.

**Table 6. Temperature Dependence of the Dose-Normalized End-of-Pulse Conductivities and Lower Limit of the Sum of the Charge-Carrier Mobilities**

| compd | temp (°C)/ sample history | $\Delta\sigma_{eop}/D$ ($10^{-9}$ Sm$^2$/J) | $\sum\mu_{min}$ [$10^{-8}$ m$^2$/(V·s)] |
|---|---|---|---|
| PPP | RT/fresh | 5.0 | 8.5 |
| PPP | 150 | 22.0 | 37.4 |
| PPP | RT/annealed | 7.5 | 12.8 |
| P3V | RT/fresh | 17.0 | 23.8 |
| P3V | 155 | 64.0 | 89.6 |
| P3V | RT/annealed | 24.0 | 33.6 |
| P2V | RT/fresh | 2.5 | 3.5 |
| P2V | 155 | 5.9 | 8.3 |
| P2V | RT/annealed | 2.5 | 3.5 |
| P5V | RT/fresh | 8.2 | 12.3 |
| P5V | 155 | 19.3 | 29.0 |
| P5V | 190 | 2.2 | 3.3 |
| P5V | RT/annealed | 3.7 | 5.5 |

**Table 7. Bandgaps of Polymers, Calculated and Measured**

| polymer | IP[a] (eV) | EA[a] (eV) | $E_g$ (eV) | 10% abs (benzene) (eV) | redox potential[b] (V) |
|---|---|---|---|---|---|
| PPP | 5.13 | −1.67 | 3.46 | 3.39 | 1.07 |
| P5V | 4.99 | −2.05 | 2.94 | 2.91 | 0.95 |
| P3V | 4.94 | −2.16 | 2.78 | 2.86 | 0.88 |
| P2V | 4.94 | −2.19 | 2.75 | 2.73 | 0.85 |
| DMeOPPV[c] | 4.72 | −2.65 | 2.07 | | 0.74[d] |
| P3A | 5.04 | −1.98 | 3.06 | 3.05 | 1.05 |

[a] Solid state values. [b] Determined by cyclovoltammetry in solution ($CH_2Cl_2$), reference: Ag/AgCl. [c] Electronic parameters calculated for planar structures. [d] Measured for diisopentoxy-PPV.

bandgaps and the experimental bandgaps, derived from the optical absorption data. The difference between the VEH P2V and P3V bandgaps is, however, too small when comparing to the one observed experimentally (0.03 eV instead of 0.13 eV). This discrepancy comes from the fact that the torsion angle of the vinylene moiety with respect to its neighboring phenylene rings in P2V should be smaller in the solid state (or even in solution) than the calculated value, which corresponds to an isolated chain (gas phase).

Table 7 also collects the results obtained in the cyclovoltammetry investigations of the PPP and PkV polymer series. The absolute values of the ionization potentials cannot be derived from these data, but the relative positions of the redox potentials for oxidation provide the evolution of the ionization potential values in the PkV series, which can then be compared to the theoretical evolution of the IP, as shown in Figure 9. A very good agreement between the experimental and

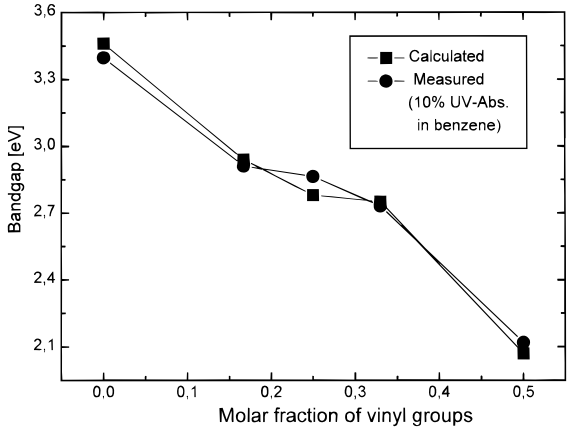


**Figure 8.** Calculated and experimental bandgap of PkV polymers plotted against the molar fraction of vinyl groups in the backbone (experimental bandgap determined as the 10% UV/vis absorption in benzene).

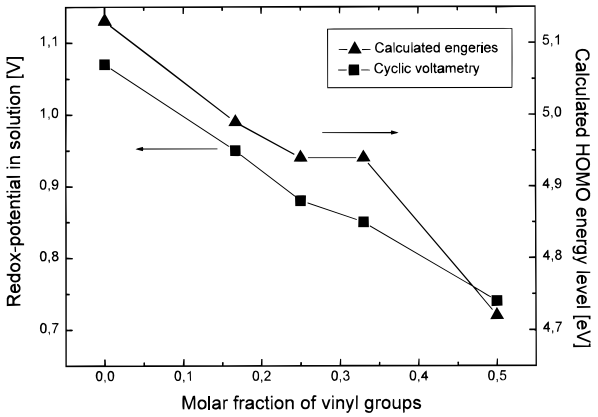


**Figure 9.** HOMO energy level of PkV polymers calculated and measured by cyclovoltammetry plotted against the molar fraction of vinyl groups in the backbone.

theoretical curves is observed, except for a small deviation obtained for the P2V ionization potential, which is calculated to be equal to the P3V value instead of being slightly smaller. This deviation can again be explained on the basis of the influence of the vinylene torsion angles on the electronic structure of P2V, as discussed above; a decrease of these dihedral angles can account for a reduction in ionization potential (as well as bandgap), as found experimentally.

From Table 7, we also note an increase in the calculated P3A ionization potential, electron affinity, as well as bandgap with respect to the P3V values. This result is a consequence of the reduction in p-conjugation due to the presence of triple bonds along the polymer backbone; this is consistent with earlier results.[53]

## IV. Discussion

**Color Tunability.** Within the different series of polymers various trends in the absorption and emission properties can be observed. In Figure 7, the energies of the absorption and emission maxima of the PkV series in the solid state are plotted against the molar fraction of vinylene units in the backbone. The PPP exhibits the highest energy of 3.70 eV (336 nm) whereas the analogous PPV has a maximum absorption of 505 nm (2.45 eV).[54] The PkV materials exhibit an absorption maximum between these two values. Upon increasing the fraction of the vinylene groups in the PPP backbone, a red shift of the absorption maximum is observed, going from 380 nm (3.26 eV) for P5V to 391 nm (3.17 eV) for

P3V and 407 nm (3.05 eV) for P2V, respectively. This trend can be described by an almost linear dependence of the maximum emission on the fraction of vinylene groups. Figure 8 shows the calculated bandgaps of the respective polymers in comparison with the experimental values. The experimental bandgap was determined at 10% of the maximum UV/vis absorption energy. Good agreement between the calculated and measured values can be observed. However, the bandgaps of the P5V and P2V are more similar to that of P3V than expected from the linear extrapolation. This leads to a plateau in Figures 8 and 9 for P2V, P3V, and P5V for the measured values of their absorption and bandgap. This deviation can be explained by the different geometries of the respective materials. From both X-ray analysis of single crystals of model compounds and oligomers[49] and computer calculations, it can be derived that the stilbene segments in all polymers are more or less planar whereas the phenyl−phenyl link shows a torsion angle of about 44°. This is an energetic compromise of the steric hindrance of the substituted phenyl rings on the one hand and the gain of conjugation by planarization of the electron-rich systems on the other hand. The rotation potential is, however, relatively weak.[55] This means that the determined torsion angle represents most likely a mean value over time than a fixed number. A deviation from the angle of 44° therefore only weakly changes the energy of the whole system, but strongly influences the conjugation and therefore the position of the electronic energy levels of the polymers. The similarity of the bandgaps of the three described polymers indicates that the stilbene unit in the PkV polymers plays a determining role for the optoelectronic properties of the material. In other words, the HOMO−LUMO separation of the polymers, e.g., of P5V, slightly varies locally along the backbone. It has a minimum in the proximity of the stilbene units in the chain and a maximum at the phenyl unit in the middle between two neighboring vinylene groups. The observed bandgap is obviously the minimum which is similar to the bandgap of P3V. In the case of P2V, the measured bandgap is slightly higher than expected. This is a consequence of the decreased interaction of two neighboring stilbene units, which cannot be planar in this polymer due to the phenyl−phenyl torsion. In P3V a planar conformation of two neighboring stilbene units is at least possible. These findings also influence the PR-TRMC measurements.

The photoluminescence emission maxima in the solid state of the PkV series exhibit similar trends. The maximum shows a red shift from 401 nm (3.09 eV, PPP) to 550 nm (2.10 eV, PPV). Therefore, the color of the emitted light can be varied to encompass a large range of the visible spectrum.

The Stokes shift of the different materials, here defined as the difference of absorption and emission maximum energies, also varies with the fraction of vinylene groups in the backbone. For PPP it is 0.61 eV whereas in PPV it is only 0.35 eV. This behavior is a consequence of the decreasing difference between the geometries of the ground and the excited state with increasing fraction of vinylene groups. The excited state of conjugated polymers tends to be more planar than the ground state.[56] Since PPV is known to be planar in the ground state and PPP is not, the decrease in Stokes shift with increasing fraction of vinylene units correlates with the presence of more planar segments in the polymer backbones.

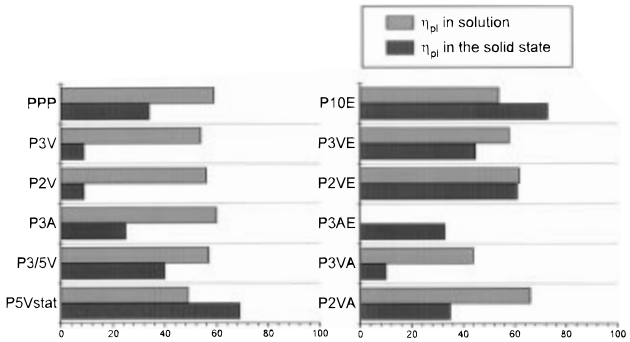


**Figure 10.** Photoluminescence quantum yields of polymers in the solid state and in solution.

Cyclovoltammetric measurements to some extent allow the experimental determination of energy levels. The differences between oxidation and reduction signals are a good measure of the bandgap and the relative position of the electronic levels of different polymers. The PkV polymers in $CH_2Cl_2$ solution showed a reversible redox potential for oxidation. A reduction peak could not be observed in any case. A comparison of the relative positions is shown in Figure 9. Again, the linear behavior is confirmed.

All observations and conclusions that were stated for the PkV series can also be made for the PkA series, which is represented by PPP and P3A. Synthesis and optical properties of poly(*p*-phenylene−ethynylene) with an analogous substitution pattern have been reported recently,[57] and the results fit perfectly into the consistent picture. The main difference to the spectral properties of the PkV series is that the PkA materials are generally blue-shifted. This is due to a decreased conjugation along the polymer backbone.

**Exciton Confinement/Mobilities.** Figure 10 compares quantum yields of photoluminescence for the homo- and copolymers as measured in dilute solution and in the solid film. The quantum yields in solution are between 43% and 66% for all homo- and copolymers. In the film a dramatic decrease in $\eta_{PL}$ is observed for all vinylene-containing homopolymers with values of approximately 10%. Contrary to this, the quantum efficiencies are above 40% for all copolymers that incorporate nonconjugated segments (P10E, P3VE, and P2VE).

Increased bulk PL quantum yields with rising fraction of nonconjugated units had been shown for derivatives of substituted poly(*p*-phenylene−vinylene).[12−14] For example, the PL efficiency in the bulk could be enhanced from 12% for the homopolymer to approximately 23% for a copolymer with a nonconjugated fraction of 38%. At the same time the photoluminescence efficiency in solution increased only by a factor of 1.33. This result indicates that the low PL quantum yields of the homopolymer in the bulk are caused by the motion of excitons to nonradiative recombination sites. Incorporation of nonconjugated segments is expected to reduce mainly the mobility of excitons along the polymer backbone. Our results are consistent with these findings. As demonstrated by the results of our pulse-radiolysis TRMC experiments (Table 5), the interruption of the conjugation decreases the charge carrier mobility by approximately 50%. Although charge carrier mobilities are not identical with exciton mobilities, the exciton can be interpreted as a bound electron/hole pair. Therefore, a certain correlation should exist between the mobilities of excitons and charge carriers.

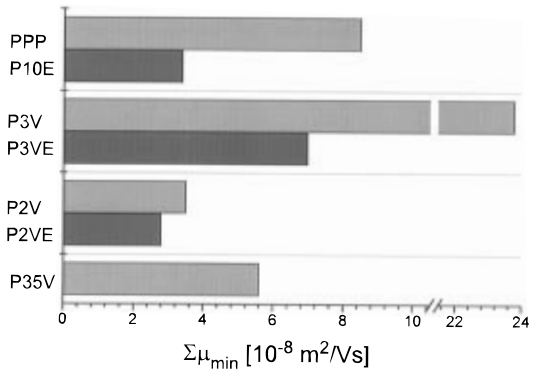


**Figure 11.** Mobilities of PkV and PkVE series, determined by pulse-radiolysis time-resolved microwave conductivity (PR-TRMC).

However, we cannot exclude that enhancement in the PL efficiency in the solid films upon incorporation of nonconjugated segments is partly caused by a reduction of the inter chain hopping rate, e.g., due to morphological changes as underlined by the microwave conductivity experiments displayed in Figure 11. For example, the incorporation of the flexible "ethylene" units into the rigid rod-like backbone will certainly reduce the stiffness of the polymer chain and thus influence the packing of adjacent molecules. Such interchain jumps will still remain possible after incorporation of nonconjugated units into the main chain—they might even be encouraged due to an altered morphology. Enhanced PL quantum yields have indeed been reported for substituted poly(thiophene) and PPV homopolymers when sufficiently long alkyl chains were attached to the polymer backbone.[6,58] This result has been explained by the dilution of the conjugated segments in the film, similar to the interpretation of the increased PL and EL efficiencies in polymer blends[16−20] or for partially converted PPV.[15]

P3/5V is a fully conjugated polymer consisting of 80% terphenylene−vinylene and 20% pentaphenylene−vinylene units. It has to be noted that P3/5V is the only material that contains a small percentage (5%) of side chains other than isopentoxy moieties. However, we do not expect this slight deviation of the chemical structure of the side-chain matrix to have any influence on the morphological, chemical, or electronic structure of the material. P3/5V is thus expected to possess a stiff polymer backbone comparable to P3V. The optical properties of the P3V and P5V homopolymers suggest that the HOMO−LUMO separation of the terphenylene−vinylene unit is only slightly smaller than the energy gap of the pentaphenylene−vinylene segments. Since the emission wavelengths of P3/5V and P3V are identical, radiative recombination must occur predominately on the P3V segments. Despite this rather small change in the chemical structure and stiffness of the polymer chain, the PL efficiency of P3/5V in the solid film is strongly enhanced by a factor of 4 compared to $\eta_{PL}$ of the P3V homopolymer (Figure 12). Similar considerations can explain why the P5V and P5Vstat or the P2V and P2VA polymers exhibit identical absorption and emission wavelengths, but very different photoluminescence quantum yields. Strong enhancement is also found in the case of an interruption of conjugation (P3VE) (Figure 12). We note that exciton Förster-type energy transfer to nonradiative sites plays a minor role. This kind of energy transfer should not be affected by slight chemical variations of the polymer backbone.

Depending on the individual comonomer solid state PL efficiencies are thus tuned over a large range without any considerable change in the emission wavelength. We have also carried out fluorescence lifetime measurements in solution and the solid state. Surprisingly, we did not find a strict correlation between the PL quantum yields and the corresponding decay times. Different mechanisms such as partial photo-oxidation or a nonunity quantum yield for singlet exciton generation have been proposed recently that might explain these findings.[60] Our results are going to be published elsewhere.

**PR-TRMC.** The dose-normalized end-of-pulse conductivity, $\Delta\sigma_{eop}/D$, in a PR-TRMC experiment is related to the sum of the mobilities of the charge carriers formed, $\sum\mu = [\mu(-) + \mu(+)]$, by

$$\Delta\sigma_{eop}/D = W_{eop}\sum\mu/E_p \tag{4}$$

In eq 4, $E_p$ is the average energy required to produce one initial ionization event, and $W_{eop}$ is the probability that an initially formed $e^-h^+$ pair survives to the end of the pulse. Since $W_{eop}$ has a maximum value of unity, a minimum value of $\sum\mu$ may be derived, if $E_p$ is known.

$$\sum\mu_{min} = E_p(\Delta\sigma_{eop}/D) \tag{5}$$

The value of $E_p$ can be estimated using the relationship derived by Alig *et al.*[59]

$$E_p \approx 2.73(E_I) + 0.5 \tag{6}$$

In eq 6, $E_I$ is the minimum energy required for ionization within a medium, i.e., the bandgap, $E_g$, for inorganic semiconductors and the ionization potential minus the electron affinity, IP − EA, for organic molecular materials. Relationship 6 is found to provide a reasonably good (±20%) approximation for $E_p$ from $E_I \approx 1$ eV for low bandgap semiconductors to $E_I \approx 8$ eV for saturated hydrocarbons. For complex media, consisting of $n$ components with an electron fraction $Z(n)$ and ionization energy $E_I(n)$, the net value of $E_I$ is given by

$$\langle E_I\rangle = \{\sum[Z(n)/E_I(n)]\}^{-1} \tag{7}$$

Values of $E_p$ have been derived for the present compounds using eqs 6 and 7 and taking $E_1 \approx E_g$, as given in Table 7, for the conjugated polymer backbone and $E_I \approx 8$ eV for the alkoxy chain component.[30] The values of $E_p$ obtained are listed in Table 4. These were used to derive the values of $\sum\mu_{min}$, which are also given in Table 4. While we cannot provide a definite upper limit to the sum of the charge-carrier mobilities, we consider it most unlikely that it would be much more than an order of magnitude larger than $\sum\mu_{min}$. We conclude, therefore, that charge-carrier mobilities in the present materials most probably lie within the range $10^{-4}$−$10^{-2}$ $cm^2/(V\cdot s)$. This is the same range that has been suggested on the basis of measurements on related poly(*p*-phenylene−vinylene) compounds.[61] Note that these values cannot be directly compared to drift mobilities as obtained by time-of-flight or transient EL experiments. Mobilities obtained by those methods might mainly be limited by charge transport across grain boundaries, whereas the microwave experiments probe a field-free and local motion of the charge carrier.

The solid samples investigated consisted of randomly oriented microdomains and probably a certain fraction of more amorphous regions. Therefore, the mobility values refer to pseudoisotropic charge migration, and

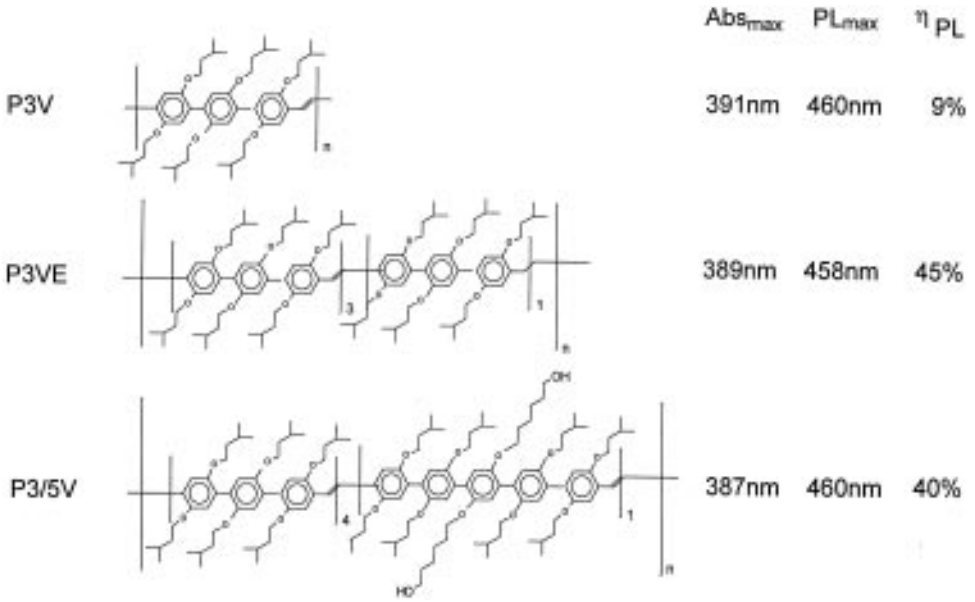


**Figure 12.** Influence of structure on optical properties: comparison of chemical structure and optical properties of P3V, P3VE, and P3/5V.

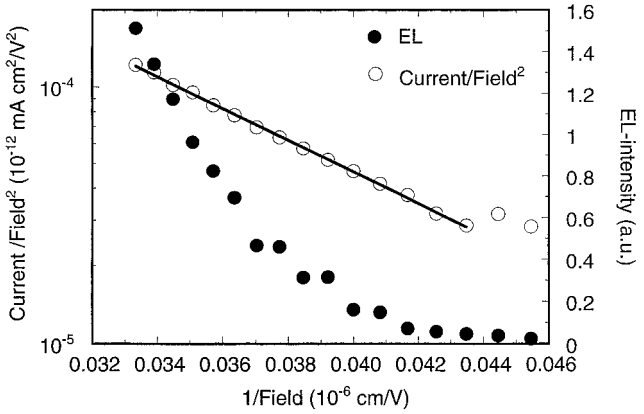


**Figure 13.** Current−voltage characteristic of an electroluminescent device (configuration: ···) fitted to the Fowler−Nordheim equation.

$\sum\mu$ will be an average value with contributions from both intrachain and interchain motion of charge carriers. The fact that $\sum\mu_{min}$ is in general lower for the compounds with ca. 10% broken conjugation suggests that the saturated ethane linkages serve as quantum barriers to intrachain charge transport and hence that this mode of transport does provide a significant contribution to the overall mobility. The substantial increase in the room temperature radiation-induced conductivity after annealing at ca. 150 °C found for PPP and P3V indicates that the morphology of the solid is of importance. This might be taken as evidence that there is also a significant contribution from interchain charge transfer to overall charge-carrier motion. Resolution of the individual contributions of intra- and interchain motion will only be possible if well aligned monodomains of the present type of material become available.

Apart from the observation that broken conjugation does in general result in a reduced charge mobility, the only other aspect which stands out is the much lower value of $\sum\mu_{min}$ for P2V than for P3V. This is of particular interest since we have found values of $\sum\mu_{min}$ for a dialkoxyphenylene−vinylene polymer ("P1V")[61] which are closer to that for P3V than P2V despite the greater structural similarity to the latter. The reason for this possibly lies in the torsional twist of 44° introduced into the polymer backbone by the biphenylene units as pointed out in a previous section. In the case of P2V, this will result in a lack of coplanarity of the vinylene units, while for P3V, coplanarity, as present in PPVs, can be restored by a second, reverse twist. This result is confirmed by the optical measurements on the bandgap of these polymers, as well as by the quantum mechanical calculations.

**Electroluminescence.** As already discussed above, the PL efficiencies in the solid state can be altered by modifying the polymer configuration. Especially the introduction of interruptions of the conjugation is accompanied by an increase of PL efficiency. It is further interesting to study the influence of the polymer configuration on the charge transport properties of the material or the balance of charges in electroluminescent devices which is reflected by the parameter *f*(el). For ladder-type PPP derivatives a significant dependence of the EL efficiency on the polymer configuration for a given PL efficiency has been reported.[29] However, since the bandgaps of the polymers investigated in this study vary by up to 0.8 eV, a substantial variation of the potential barrier for charge-carrier injection has to be expected. Therefore, *f*(el) is not only a function of the conditions for charge transport in the polymers.

Tables 2 and 4 show that three types of materials can be identified. The first group consists of PPP and P10E, which possess the largest bandgap of the series of $E_g$ = 3.75 eV. Here the efficiencies of single-layer devices are relatively small, *f*(el) = 0.1−0.5%, as calculated from the ratio of the EL internal efficiency and the PL quantum yields according to eq 2. The second group consists of polymers which have bandgaps around $E_g$ = 2.75 eV. Here, *f*(el) = 1.1−1.6%, and single-layer efficiencies up to 0.24% are achieved. The second group is formed by P2V and P3A, which show values for *f*(el) of 2.0−4.8% and have the smallest bandgaps of $E_g$ = 2.5 eV.

The *f*(el) values for triple-layer devices indicate a good balance of hole and electron current. In these devices the recombination probability *r* for electrons should be close to unity, so that *r* does not vary significantly for the different polymers. It is therefore most likely that

the observed trends of *f*(el) for the different device configurations are caused by the varying height of the injection barrier for electrons, which reduces the device efficiency most for devices with high bandgap. These findings are consistent with the results of the PR-TRMC experiments, where only moderate variations of the sum of the mobilities of charge carriers for the different polymers are found. Especially the results obtained with group two (Table 4) indicate that the relative contributions of holes and electrons does not vary significantly with the specific polymer configuration.

MEH-PPV has the lowest bandgap of 2.1 eV and corresponds to a *f*(el) = 40% and an EL efficiency of about 1% in single-layer devices. Here the position of the HOMO and LUMO and the conversion of charge carriers into optical excitations are nearly optimized in a typical device structure.[25]

Devices which include an additional HTL of PVK do not show a substantial increase of EL efficiency. It has been shown, recently, that the LUMO of PVK is located at about 1.2 eV.[62] If the device current were dominated by electrons, a blocking of electrons at the PVK/polymer interface with a subsequent improvement of charge-carrier balance and device efficiency would have to be expected. Therefore, the device current is more likely to be dominated by holes. The only small differences in the EL efficiencies of bilayer and corresponding monolayer devices show that the effect of the additional PVK layer on hole injection and transport is less pronounced than stated by Parker et al.[62] However, an increase of the overall film thickness can already increase the device efficiency by moving the recombination zone further away from the top electrode, where luminescence quenching due to near-field coupling of the exciton to the metal has to be expected.

An exception is formed by PPP, which gives relatively inefficient single-layer devices. This could be result of a higher ionization potential and therefore higher injection barrier for holes, compared with the HTL. However, PPP single-layer devices are not very stable and tend to exhibit strong current anormalies. Devices containing an additional HTL show increased device stability. We attribute this effect to a blocking of charge tranport through channels such as filaments or grain boundaries, that do not contribute to the light emission. P10E has the same bandgap and shows one of the highest PL efficiencies of the series with a comparable efficiency already in single-layer devices.

Triple-layer devices containing both a HTL and an ETL show the highest increase of efficiency of typically more than an order of magnitude compared to the single-layer device. This confirms the assumption of a hole-dominated current, which is reduced by the blocking of holes at the polymer/ETL interface. A comparison of the calculated positions of LUMO and HOMO for the polymers and PBD (see Figure 14) shows that a significant potential step for the holes at the interface has to be expected. This effect has been described in the literature before[26] and is a widely used tool for the optimization of luminescent devices.[25] The distribution of the obtained values for *f*(el) in the triple-layer devices is comparable to the single-layer devices.

For most devices the onset field for EL is reduced for devices which contain the ETL. This might be due to a lower position of the LUMO of the ETL for most polymers, which could facilitate electron injection into the device and therefore shift the light onset field to lower values. The increase of device efficiency is the highest for PPP, which is a consequence of the reasons explained above.

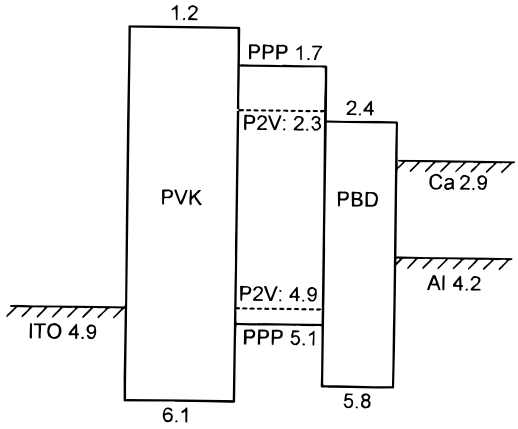


**Figure 14.** Energy levels of different layers and electroluminescent multilayer devices.

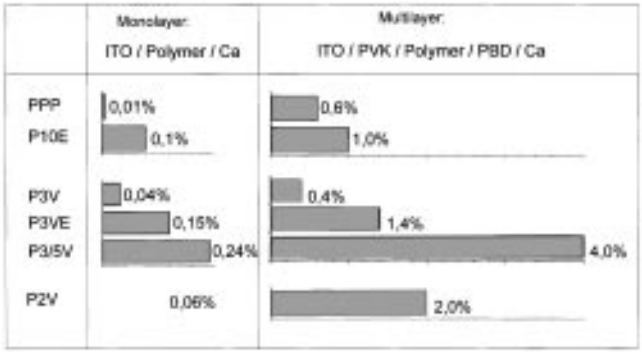


**Figure 15.** Internal quantum efficiencies of different device configurations of polymers.

We find no evidence for a reduction of device efficiency due to interfacial exciton splitting, which is consistent with the fact that the offset of the LUMOs of the polymers and PBD is only of the order of some 0.1 eV. If the difference of the electron affinity of PBD and the polymers were larger than the exciton binding energy, electron transfer to the PBD could be energetically favored.

For voltages above light onset, the current−voltage characteristics of the devices in forward bias can typically be described by a Fowler−Nordheim profile (see Figure 13). This indicates that at high bias the device current is limited by tunnel injection, which is consistent with earlier studies of polymer light-emitting devices.[25,29]

Further evidence for the confinement of charge carriers at the polymer/ETL interface can be obtained from the EL spectra. As outlined above, the EL spectra of devices containing an ETL are rather similar to the PL spectrum, but the emission from single- or double-layer devices containing an HTL exhibits an additional red-shifted contribution. This is most distinct in devices which contain P3A. This effect could be explained, if we assume that a small concentration of additional lumophores exist in these materials. These could be formed by a limited degree of molecular aggregation or by other kinds of intragap trap levels. Emission from these sites is not observed in the PL experiment, which is probably due to their small concentration and a limited diffusion range of the excitons. However, in the EL the transfer of charge carriers might preferably probe these sites, e.g., due to trapping. EL might also be generated by electrons and holes which both pen-

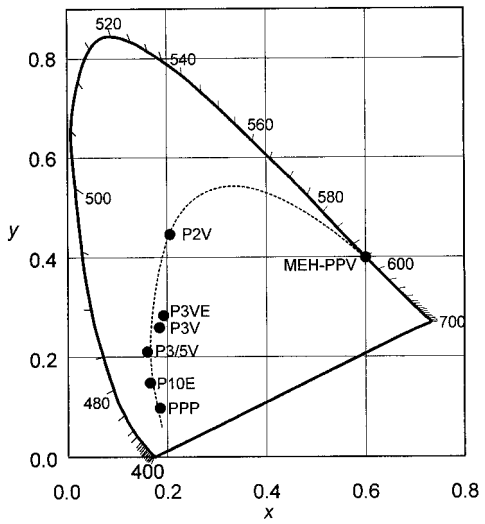


**Figure 16.** Localization of the electroluminescence spectra of various polymers in the Maxwell triangle.

etrate into the polymer in devices containing an HTL. It has been shown in the literature that the recombination zone in a polymer light-emitting device can extend over a major part of the polymer layer.[63] The situation might be reversed for devices containing an ETL which exhibit a significant degree of charge-carrier confinement. In this case the penetration depth of the electrons into the polymer film is limited due to the high density of the holes at the polymer/ETL interface and the relative positions of the LUMOs. Holes which are trapped in the polymer layer are therefore less likely to contribute to the EL, and the situation of the generation of excitons is comparable to the PL. It might also reflect the fact that in conjugated organic materials electrons are typically less mobile than holes because of a higher trap density for electrons than for holes.[64] Again the P3A triple-layer device shows limited amount of red-shifted emission, which might reflect the longer penetration depth of the electrons.

The red-shifted contribution generally increases with operation time because of the generation of low lying states possibly caused by aggregation or degradation. A different effect causing low lying states in the material might be a specific polymer−metal interaction. Note that the red-shifted contributions were most pronounced in P3A devices with a direct polymer−calcium interface. A certain chemical interaction of the metal with the triple bonds of this polymer might therefore be the reason for the observed strong red shift.

Figure 16 shows the coordinates of the EL emission spectra of various polymers in the Maxwell triangle. The emission of the different PkV and PkVE polymers can be localized on a line ranging from the deep and pure blue of the PPP to a red emission of the analogous substituted PPV.

In summary, the EL investigations show that the current in single-layer devices is dominated by holes. The results achieved with single- and multilayer devices are consistent with the calculated HOMO and LUMO of the polymers. The molecular structure does not significantly influence the charge-carrier balance, which is rather defined by the injection condition for electrons and holes. Since the mobility for charges under high bias is probably higher, the combination of inter- and intrachain charge transport also might neutralize the effect of molecular sites which show exciton confinement.

## V. Conclusion

We have presented a variety of new PPP-related polymers. Using a new synthetic approach, the chemical structure of the polymer backbone can be tailored. The materials exhibit molecular weights above 10 000 g/mol. All polymers show similar phase behavior: a glass transition is observed at about 20−40 °C and the materials melt at temperatures between 190 and 250 °C to form an anisotropic liquid phase.

Both maximum absorption and emission can be tailored in various polymer series to encompass a large range of the visible spectrum. The localization of the energy levels of the polymers has been determined with quantum mechanical calculations and experimentally with optical methods and cyclovoltammetry. The measurements agree well with the calculated values of the relative positions of the energy levels. A linear decrease of the bandgap with increasing fraction of vinylene moieties in a PPP backbone is observed.

Photoluminescence quantum yields of all polymers in solution are between 43% and 62%. PL quantum yields in the solid state are strongly influenced by slight variations of the backbone. If the conjugation of the backbone is interrupted by nonconjugated units or the local electronic structure of the polymer is altered, the PL efficiences in the solid state strongly increase up to 73%. However, shape and position of the absorption and emission spectra remain unchanged. This strong increase of PL efficiency upon slight changes in the chemical structure might be explained by a decreased exciton mobility or by an increased quantum yield for the photogeneration of singlet excitons.

The mobilities of charge carriers measured in the microwave conductivity experiment are on the order of $10^{-7}$ $m^2/(V \cdot s)$ with an activation energy of ca. 0.06 eV. If the conjugation is interrupted every tenth phenyl unit, mobilities are reduced by a factor of about 2. A substantial increase in the room temperature radiation-induced conductivity after annealing at ca. 150 °C indicates that the morphology of the solid is of importance. This might be taken as evidence that there is a significant contribution from interchain charge transfer to the overall charge-carrier motion.

Various EL devices in single-, double-, and triple-layer configurations with electron- and hole-transporting layers (PBD, PVK) show that the EL emission colors can be widely varied from 410 nm to approximately 500 nm. Generally, the current through the device is dominated by the holes. Introduction of a PBD electron-transport layer between the light-emitting polymer and the anode leads to a more balanced charge injection and thus increases the internal quantum efficiency of electroluminescence. At this same time, the onset field for light emission is significantly reduced in that case, too. The major effect of a PVK layer is the blocking of charge transport through channels such as filaments or grain boundaries which do not contribute to the light emission. Surprisingly, single-layer and triple-layer devices from the same emitting polymer showed distinct variations in the EL spectra, which could be explained by different charge transport and trapping mechanism in the multilayer structures.

EL efficiencies of the new materials are generally very large. Values of up to 4% in the blue region have been achieved in triple-layer devices. In general, the EL efficiencies correlated well with the PL quantum yields in the solid films. However, a comparison of EL and

PL efficiencies shows that balanced charge injection has so far not been achieved for most systems.

**Acknowledgment.** M.R. gratefully acknowledges support by Kékule scholarship of the Stiftung Stipendienfonds des Verbandes der chemischen Industrie. The authors would like to thank G. Wegner, V. Cimrová, and M. Schulze for helpful discussions. The work in Mons is partly supported by the European Commission (ESPRIT Project LEDFOS-8013), the Belgian Prime Minister Office of Science Policy (SSTC) "Pôle d'Attraction Interuniversitaire en Chimie Supramoléculaire et Catalyse", FNRS/FRFC, and an IBM Academic Joint Study.

## References and Notes

(1) Burroughes, J. H.; Bradley, D. D. C.; Braun, A. R.; Marks, R. N.; Mackay, K.; Friend, R. H.; Burn, P. L.; Holmes, A. B. *Nature* **1990**, *347*, 539.
(2) Karg, S.; Riess, W.; Dyakonov, V.; Schwoerer, M. *Synth. Met.* **1993**, *54*, 427.
(3) Grem, G.; Leditzky, G.; Ullrich, B.; Leising, G. *Synth. Met.* **1992**, *51*, 383.
(4) Grem, G.; Leising, G. *Synth. Met.* **1993**, *55*−*57*, 4105. Yang, Y.; Pei, Q.; Heeger, A. J. *J. Appl. Phys.* **1996**, *79*, 934.
(5) Ohmori, Y.; Uchida, M.; Muro, K.; Yoshino, K. *Solid State Commun.* **1991**, *80*, 605.
(6) Doi, S.; Kuwabara, M.; Noguchi, T.; Ohnishi, T. *Synth. Met.* **1993**, *550*−*57*, 4174.
(7) Berggren, M.; Inganäs, O.; Gustafsson, G.; Rasmusson, J.; Andersson, M. R.; Hjertberg, T.; Wennerström, O. *Nature* **1994**, *372*, 444.
(8) Gill, R. E.; Malliaras, G. G.; Wildeman, J.; Hadziioannou, G. *Adv. Mater.* **1994**, *6*, 132.
(9) Zyung, T.; Hwang, D.-H.; Kang, I.-N.; Shim, H.-K.; Hwang, W.-Y.; Kim, J.-J. *Chem. Mater.* **1995**, *7*, 1499.
(10) Malliaras, G. G.; Herrema, J. K.; Wildeman, J.; Wieringa, R. H.; Gill, R. E.; Lampoura, S. S.; Hadziioannou, G. *Adv. Mater.* **1993**, *5*, 721.
(11) Herrema, J. K.; van Hutten, P. F.; Gill, R. E.; Wildeman, J.; Wieringa, R. H.; Hadziioannou, G. *Macromolecules* **1995**, *28*, 8102.
(12) Burn, P. L.; Holmes, A. B.; Kraft, A.; Bradley, D. D. C.; Brown, A. R.; Friend, R. H.; Gymer, R. W. *Nature* **1992**, *356*, 47.
(13) Staring, E. G. J.; Demandt, R. C. J. E.; Braun, D.; Rikken, G. L. J.; Kessener, Y. A.-R. R.; Venhuizen, A. H. J.; Wynberg, H.; ten Hoeve, W.; Spoelstra, K. J. *Adv. Mater.* **1994**, *6*, 934.
(14) Braun; D.; Staring, E. G. J.; Demandt, R. C. J. E.; Rikken, G. L. J.; Kessener, Y. A.-R.R.; Venhuizen, A. H. J. *Synth. Met.* **1994**, *66*, 75.
(15) Zhang, C.; Braun, D.; Heeger, A. J. *J. Appl. Phys.* **1993**, *73*, 5177.
(16) Vestweber, H.; Greiner, A.; Lemmer, U.; Mahrt, R. F.; Richert, R.; Heitz, W.; Bässer, H. *Adv. Mater.* **1992**, *4*, 661. Vestweber, H.; Oberski, J.; Greier, A.; Heitz, W.; Mahrt, R. F.; Bässler, H. *Adv. Mater. Opt. Electron.* **1993**, *2*, 197.
(17) Pommerehne, J.; Vestweber, H.; Guss, W.; Mahrt, R. F.; Bässler, H.; Porsch, M.; Daub, J. *Adv. Mater.* **1995**, *7*, 551.
(18) Yu, G.; Nishino, H.; Heeger, A. J.; Chen, T.-A.; Rieke, R. D. *Synth. Met.* **1995**, *72*, 249.
(19) Kang, I.-N.; Hwang, D.-H.; Shim, H.-K.; Zyung, T.; Kim, J.-J. *Macromolecules* **1996**, *29*, 165.
(20) Zhang, C.; von Seggern, H.; Kraabel, B.; Schmidt, H.-W.; Heeger, A. J. *Synth. Met.* **1995**, *72*, 185.
(21) Cimrová, V.; Remmers, M.; Neher, D.; Wegner, G. *Adv. Mater.* **1996**, *8*, 146.
(22) Lemmer, U.; Heun, S.; Mahrt, R. F.; Scherf, U.; Hopmeier, M.; Siegner, U.; Göbel, E. O.; Müllen, K.; Bässler, H. *Chem. Phys. Lett.* **1995**, *240*, 373.
(23) Remmers, M.; Schulze, M.; Wegner, G. *Macromol. Rapid Commun.* **1996**, *17*, 239.
(24) Greenham, N. C.; Friend, R. H.; Bradley, D. D. C. *Adv. Mater.* **1994**, *6*, 491.
(25) Parker, I. *J. Appl. Phys.* **1994**, *75*, 1656.
(26) Brown, A. R.; Greenham, N. C.; Burroughes, J. H.; Bradley, D. D. C.; Friend, R. H.; Burn, P. L.; Kraft, A.; Holmes, A. B. *Appl. Phys. Lett.* **1992**, *61*, 46.
(27) Rauscher, U.; Bässler, H.; Bradley, D. D. C.; Hennecke, M. *Phys. Rev. B* **1990**, *42*, 9830.
(28) Vestweber, H.; Bässler, H.; Grüner, J.; Friend, R. H. *Chem. Phys. Lett.* Submitted.
(29) Grüner, J.; Hamer, P.; Friend, R. H.; Huber, J.; Scherf, U.; Holmes, A. B. *et al. Adv. Mater.* **1994**, *6*, 748.
(30) Schouten, P. G. Ph.D. Thesis, Delft University of Technology, Delft, 1994, ISBN 90-73861-22-5.
(31) Warman, J. M.; Haas, M. P. In *Pulse Radiolysis of Irradiated Systems*; Tabata, Y., Ed.; CRC Press: Boca Raton, FL, 1991; pp 101−133; ISBN 0-8493-4881-1.
(32) Dewar, M. J. S.; Zoebisch, E. J.; Healy, E. F.; Stewart, J. J. P. *J. Am. Chem. Soc.* **1985**, *107*, 3902.
(33) Lhost, O.; Bredas, J. L. *J. Chem. Phys.* **1992**, *96*, 5279.
(34) Brédas, J. L.; Chance, R. R.; Silbey, R.; Nicolas, G.; Durand, Ph. *J. Chem. Phys.* **1981**, *75*, 255.
(35) Brédas, J. L.; Chance, R. R.; Silbey, R.; Nicolas, G.; Durand, Ph. *J. Chem. Phys.* **1982**, *77*, 371.
(36) Vanhee, S.; Rulkens, R.; Lehmann, U.; Rosenauer, C.; Schulze, M.; Köhler, W.; Wegner, G. *Macromolecules*, in press.
(37) Wegner, G. *Thin Solid Films* **1992**, *216*, 105.
(38) Wegner, G. *Mol. Cryst. Liq. Cryst.* **1993**, *235*, 1.
(39) Rulkens, R.; Schulze, M.; Wegner, G. *Macromol. Chem.; Rapid Commun.* **1994**, *15*, 669.
(40) Grimme, J.; Kreyenschmidt, M.; Uckert, F.; Müllen, K.; Scherf, U. *Adv. Mater.* **1995**, *7*, 292.
(41) Cumpston, B. H.; Jensen, K. F. *Synth. Met.* **1995**, *73*, 195.
(42) Montaudo, G.; Vitalini, D.; Lenz, R. W. *Polymer* **1987**, *28*, 837.
(43) Witteler, H.; Lieser, G.; Wegner, G.; Schulze, M. *Macromol. Chem.; Rapid Commun.* **1993**, *14*, 471.
(44) Vahlenkamp, T.; Wegner, G. *Macromol. Chem. Phys.* **1994**, *195*, 1933.
(45) Ballauff, M. *Macromolecules* **1986**, *19*, 1366.
(46) Remmers, M.; Wegner, G. To be published.
(47) Schuddeboom, W. Ph.D. Thesis, Delft University of Technology, 1994, ISBN 90-73861-21-7.
(48) Delugeard, Y.; Desuche, J.; Baudour, J. L. *Acta Crystallogr., Sect. B* **1976**, *32*, 702. Baudour, J. L.; Delugeard, Y.; Rivet, P. *Ibid.* **1978**, *34*, 625. Baker, K. N.; Knachel, H. C.; Fratini, A. V.; Adams, W. W. *Mater. Res. Soc. Symp. Proc.* **1989**, *134*, 497. Bastiansen, O.; Samdal, S. J. *J. Mol. Struct.* **1985**, *128*, 115.
(49) Remmers, M.; Enkelmann, V.; Wegner, G. To be published.
(50) Meyers, F.; Heeger, A. J.; Brédas, J. L. *J. Chem. Phys.* **1992**, *97*, 2750. Quattrocchi, C.; dos Santos, D. A.; Brédas, J. L. *Synth. Met.* **1995**, *74*, 187.
(51) Meyers, F.; Heeger, A. J.; Brédas, J. L. *J. Chem. Phys.* **1992**, *97*, 2750.
(52) dos Santos, D. A.; Quattrocchi, C.; Friend, R. H.; Brédas, J. L. *J. Chem. Phys.* **1994**, *100*, 3301. Quattrocchi, C.; dos Santos, D. A.; Brédas, J. L. *Synth. Met.* **1995**, *74*, 187.
(53) Geisler, T.; Dehu, C., *et al. J. Phys. Chem.* **1994**, *98*, 10102.
(54) Wittmann, H. F.; Grüner, J.; Friend, R. H.; Spencer, G. W. C.; Moratti, S. C.; Holmes, A. B. *Adv. Mater.* **1995**, *7*, 541.
(55) Hofmann, H.-J.; Köhler, H.-J.; Thieroff, K.; Uhlmann, P. *J. Prakt. Chem.* **1974**, *316*, 639. Hofmann, H.-J.; Birner, P. *Z. Chem.* **1975**, *15*, 23.
(56) Momocchillie, F.; Bruni, M. C.; Baraldi, I. *J. Phys. Chem.* **1972**, *76*, 3983. Gustav, K.; Sühnel, J.; Wild, U. P. *Helv. Chim. Acta* **1978**, *61*, 2100.
(57) Moroni, M.; Le Moigne, J.; Luzatti, S. *Macromolecules* **1994**, *27*, 562.
(58) Greenham, N. C.; Brown, A. R.; Bradley, D. D. C.; Friend, R. H. *Synth. Met.* **1993**, *55*−*57*, 4134.
(59) Yan, M.; Rothberg, L. J.; Papadimitrakopoulos, F.; Galvin, M. E.; Miller, T. M. *Phys. Rev. Lett.* **1994**, *72*, 1104.
(60) Alig, R. C.; Bloom, S.; Struck, C. W. *Phys. Rev. B* **1980**, *22*, 5565.
(61) Gailberger, M.; Bässler, H. *Phys. Rev. B* **1991**, *44*, 8643. Gelinck, G. H.; Warman, J. M.; Staring, E. G. J. To be published. Takiguchi, T.; Park, D. H.; Ueno, H.; Yoshino, K.; Sugimoto, R. *Synth. Met.* **1987**, *17*, 657−662. Bradley, D. D. C.; Shen, Y. Q.; Bleier, H.; Roth, S. *J. Phys. C: Solid State Phys.* **1988**, *21*, L515−522.
(62) Parker, I. D.; Pei, Q. *Appl. Phys. Lett.* **1994**, *65*, 1272.
(63) Brown, A. R.; Greenham, N. C.; Burroughes, J. H.; Bradley, D. D. C.; Friend, R. H.; Burn, P. L.; Kraft, A.; Holmes, A. B. *Chem. Phys. Lett.* **1992**, *200*, 46. Vestweber, H.; Sander, R.; Greiner, A.; Heitz, W.; Mahrt, R. F.; Bässler, H. *Synth. Met.* **1994**, *64*, 141.
(64) Marks, R. N., *et al. J. Phys.: Condens. Matter* **1994**, *6*, 1379.

MA960599G